J Mater Sci (2009) 44:3800–3806
DOI 10.1007/s10853-009-3513-9

Influence of different deformation processing on the AZ31 magnesium alloy sheets

Su-Qin Zhu · Hong-Ge Yan · Wei-Jun Xia · Ji-Zi Liu · Jun-Feng Jiang

Received: 19 March 2009 / Accepted: 22 April 2009 / Published online: 7 May 2009
© Springer Science+Business Media, LLC 2009

Abstract AZ31 magnesium alloy sheets were processed by normal rolling (NR), one-pass equal channel angular rolling (1P-ECAR), and cross equal channel angular rolling (C-ECAR) at 400 °C on a die with 105 ° channel angle. The microstructure, texture, and tensile properties of sheets were measured. The results show that ECAR processing can weaken the basal plane texture, thus obviously improve the mechanical properties. The yield ratio σ_s/σ_b decreases and strain hardening exponent n increases along rolling direction (RD) during ECAR, which means that the uniform plastic formability is enhanced. After C-ECAR, the mechanical properties along both the RD and transverse direction (TD) are improved. Different twinning types, fine $\{10\bar{1}1\}$ contraction twinning in the NRed sheets and coarse $\{10\bar{1}2\}$ extension twinning in the ECARed sheets, were observed. The easier activation of $\{10\bar{1}2\}$ twinning and basal $\langle a \rangle$ slip leads to the lower yield strength of the ECARed sheets. Dynamic recrystallization (DRX) during the rolling process has great effect on the microstructure of the as-deformed and annealed sheets. The annealed C-ECARed sheets have significant finer and homogenous grains than the annealed NRed sheets, which is attributed to the rarely DRX process during ECAR. The average grain sizes of the annealed C-ECARed samples and NRed samples are 14 and 24 μm, respectively.

S.-Q. Zhu · H.-G. Yan (✉) · W.-J. Xia · J.-Z. Liu · J.-F. Jiang
College of Materials Science and Engineering,
Hunan University, Changsha, 410082 Hunan, China
e-mail: sqzhu222@yahoo.com.cn

Introduction

Magnesium and its alloys have great potential in the fields of automobile, aerospace, electronics etc., due to their low-density, high-specific strength and stiffness, excellent castability and damping characteristics, and good electromagnetic shielding ability. However, low-ductility at ambient temperature limits their industrial applications owing to the hcp structure [1–4]. In recent years, numerous measures have been taken to enhance the ductility, one important method of which is severe plastic deformation (SPD) technique, including equal channel angular extrusion or pressing (ECAE or ECAP), high pressure torsion (HPT), cyclic extrusion compression (CEC), accumulative roll bonding (ARB), multiple forging (MF), repetitive corrugation and straightening (RCS), etc. [5–11]. These techniques have been used to produce ultrafine-grained (UFG) materials along with texture variation to improve the formability of magnesium alloys, even the superplasticity at low temperature and high-strain rate was obtained [12, 13].

A novel SPD technique, so-called continuous confined strip shearing (C2S2) or equal channel angular rolling (ECAR) based on ECAE, has been developed by Lee et al. [14–19] to process aluminum alloy and steel sheets with microstructure of uniform fine grains and large portion of high-angle grain boundaries (HAGBs). During C2S2 processing, shear stress was applied to the sheets. The available results show that this processing can also be used to weaken the texture of the sheets.

The present study concerns a new equal channel angular rolling (ECAR) processing developed by our team formerly [20–23]. This study used normal rolling and different ECAR processes to produce AZ31 magnesium sheets, and the aim is to investigate the influence of different deformation

processing on the microstructures including twinning characteristics, texture, and mechanical properties.

Experimental procedure

The ECAR die used to produce magnesium alloy sheets in this study is shown in Fig. 1, which is different from the C2S2 die [14]. Shear stress will be applied to the sheet via the die channel. The channel angle (θ) is 105°. The twin-rolls are conventional without any special design.

The initial material was a cast billet of AZ31 alloy (nominally Mg-3 Al-1 Zn-0.3 Mn in wt%) homogenized at 370 °C for 4 h. The billet of 160 mm in diameter was hot extruded at 300 °C to a rectangular bar with dimensions of 10×120 mm^2, at an extrusion ratio of 17.8. Then the as-extruded bar was normally rolled (denoted as NR) to sheets with thickness of 2 mm with reduction per pass 15–20%. Then the NRed sheets were ECARed one pass along the previous RD (rolling direction) (denoted as 1P-ECAR), i.e., the 1P-ECARed and NRed sheets have the same RD and TD (transverse direction). And then the 1P-ECARed sheets were rotated 90° in the RD–TD plane followed by ECAR for another pass (named as cross equal channel angular rolling, denoted as C-ECAR), i.e., the RD of the C-ECARed sheets is the TD of the previous 1P-ECARed sheets. In order to eliminate the strain hardening, the as-extruded bar, NRed sheets and 1P-ECARed sheets were heated at 400 °C for 10 min before NR, 1P-ECAR, and C-ECAR, respectively. And the sheets were intermediately re-heated at 400 °C for 5 min between normal rolling passes. Some of the NRed, 1P-ECARed, and C-ECARed sheets were annealed at 300 °C for 30 min for microstructure investigation and tensile test.

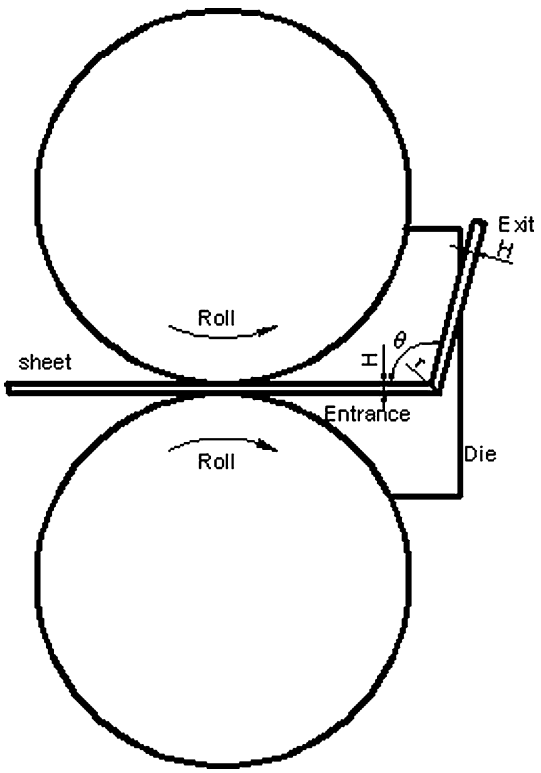

Fig. 1 A schematic illustration of ECAR process

The metallographic microstructures of the sheets before and after annealing were observed by optical microscopy. The samples were mechanically ground and polished, then etched in acetic picral. The twin morphology and selected area diffraction (SAD) of the NRed and C-ECARed samples were measured on JEOL-3010 HRTEM. The TEM samples were mechanically ground and polished below 100 μm, then punched to ∅ 3 mm foils, followed by twin-jetting in an electrolyte of 5.3 g lithium chloride, 11.16 g dehydrite, 500 mL methanol, and 100 mL 2-butoxyethanol. The NRed, 1P-ECARed, and C-ECARed samples with 10×10 mm^2 were polished to mid-layer to measure texture at a D8 DISCOVER X-ray Diffractometer. And the tensile samples were linear cut from the as-rolled sheets with the gauge length of 15 mm. The tensile test was carried out on a WDW-100 universal testing machine at ambient temperature, with initial strain rate of 5.6×10^{-4} s^{-1}. The fracture images of the tensile samples were observed on a JSM-6700F SEM.

Results and discussion

Microstructure

The metallographic microstructures of the as-rolled and annealed sheets are shown in Figs. 2 and 3. The grain size distributions in the three as-rolled sheets are inhomogeneous, with lots of curved grain boundaries, which is a typical deformed microstructure of magnesium alloys. The average grain sizes of the NRed, 1P-ECARed, and C-ECARed samples are 18, 19, and 19 μm, respectively. Grain refinement was not observed after ECAR processing. The recrystallization temperature of the deformed AZ31 alloy is below 300 °C, while the sheets were re-heated at 400 °C for 10 min before each pass during ECAR, which could lead to grain growth and results in the weakening of grain refinement effect of SPD. On the other hand, the UFG structure could be obtained only if the strain imparted to the specimen per pass and the accumulative strain exceed to certain values during C2S2 according to Ref. [15].

It's evident that dynamic recrystallization (DRX) occurred during NR from Fig. 2a. However, the DRX is obviously incomplete, which leads to the heterogeneous microstructure. In the DRX region, twins disappeared. Thus, during the subsequent annealing at 300 °C, grains in

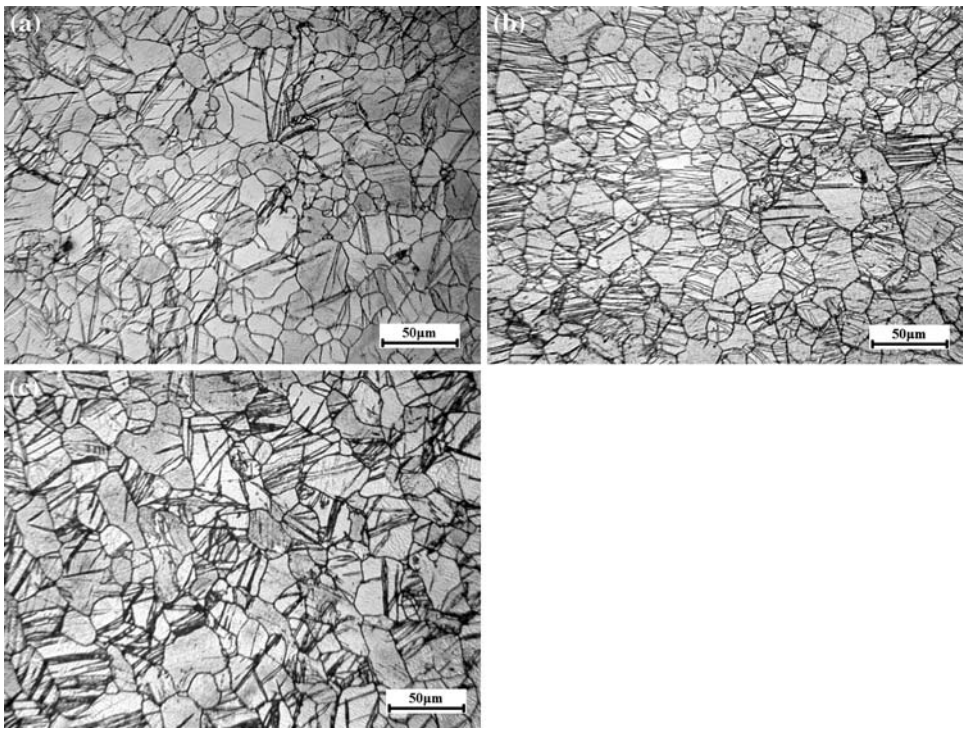

Fig. 2 The optical micrographs of **a** NRed **b** 1P-ECARed **c** C-ECARed sheets (RD–TD plane)

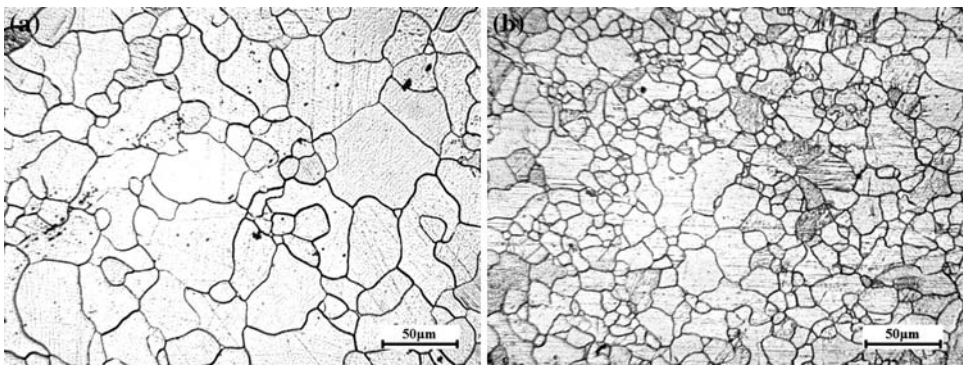

Fig. 3 The optical micrographs of **a** NRed **b** C-ECARed sheets after annealing at 300 °C for 30 min (RD–TD plane)

the DRXed region almost without any defect might grow coarser directly. While in the as-deformed region without DRX, more defects such as dislocation piles-up and twins will be the nucleus of static recrystallization (SRX), and grains growing from these new nucleus will be significantly finer than the grains growing directly, resulting in the inhomogenous microstructure in the NRed samples after annealing, as shown in Fig. 3a. In contrast, DRX rarely occurs in the ECARed samples and twins appear in nearly every grain, which is caused by the lower temperature of the cold die and lubricant, as seen in Fig. 2b and c. The rare DRX process would be another reason for the non-refinement effect on the grain size during ECAR. Therefore, the SRX nucleus initiating from the as-deformed microstructure in the ECARed samples will be more and uniform, which results in the finer and homogenous grains, as shown in Fig. 3b. As seen in Fig. 3, after annealing at 300 °C for 30 min, twins almost disappear in both the NRed and C-ECARed sheets. The average grain size of the annealed C-ECARed samples is 14 μm, significantly finer than that of the annealed NRed samples, which is 24 μm. It can be concluded that DRX during the rolling process has great effect on the microstructure of the as-deformed and annealed sheets.

It can be seen from Fig. 2 that a large amount of twins appeared in all the three samples. Most twins in the NRed samples are fine, except a few coarser ones in some grains. And twins in the ECARed samples are almost all coarse with lens morphology. Figure 4 shows the HRTEM images of the NRed and C-ECARed samples and the SAD pattern of the matrix and twin in each sample. The diffraction spots were separated into two parallelograms, which are the diffractions of matrix (subscript M in Fig. 4) and twin (subscript T in Fig. 4), respectively. The shared spot of the

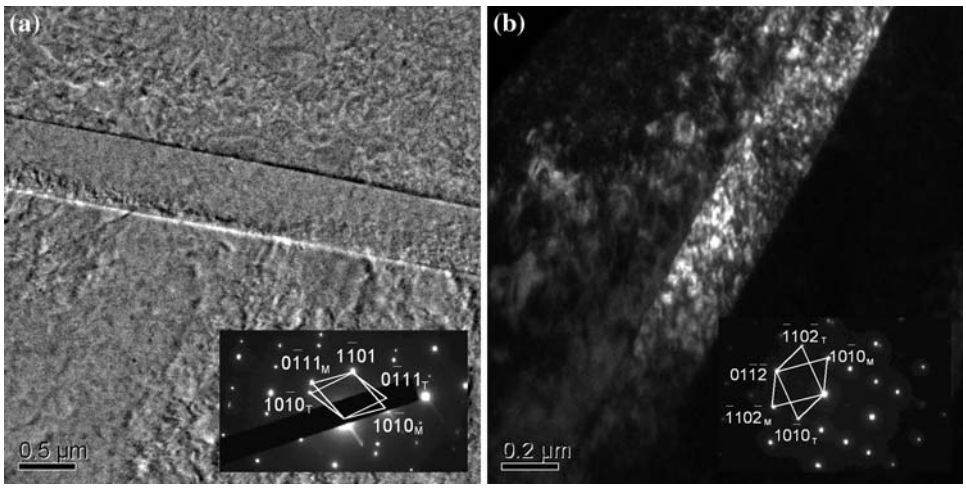

Fig. 4 The HRTEM images and SAD patterns of **a** NRed (*bright field*) **b** C-ECARed sample (*dark field*)

two parallelograms indicates the twinning plane. It is found that $\{10\bar{1}1\}$ contraction twinning appears in the NRed sheets and $\{10\bar{1}2\}$ extension twinning appears in the C-ECARed sheets according to the diffraction patterns. Considering with the optical microstructures and SAD patterns simultaneously, $\{10\bar{1}1\}$ and $\{10\bar{1}2\}$ twins correspond to the finer twins in the NRed samples (see Fig. 2a) and the coarser twins in the ECARed samples (see Fig. 2b, c), respectively. That is, the $\{10\bar{1}1\}$ twinning occurs most frequently in the NRed sheets, and $\{10\bar{1}2\}$ twinning occurs in the ECARed sheets. Furthermore, there are high density dislocations in both twin and matrix.

Texture

The NRed sheets showed a severe basal plane texture, which is the typical rolling texture with (0002) basal planes parallel to the rolling plane, as shown in Fig. 5a. 1P-ECAR process leads to the wider spread of the basal planes to RD, and the maximum pole density decreases from 14.71 to 13.18. While after C-ECAR process, the spread of the basal planes becomes substantially broader to TD, along with notable decrease in pole density with maximum 6.03. It could be concluded that ECAR reorients the grains and makes the basal planes rotate a certain degrees from the rolling plane, resulting in a marked weakening of the basal plane texture.

Mechanical properties

The true stress and true strain curves of the annealed NRed, 1P-ECARed, and C-ECARed samples tensioned in RD and TD during the uniform plastic deformation are shown in Figs. 6 and 7, respectively. The tensile data are given in Table 1, containing yield strength σ_s, tensile strength σ_b, elongation δ, yield ratio σ_s/σ_b and strain hardening exponent n. It can be seen that both σ_s and σ_b of the sheets decreases, while the δ increases after ECAR. After

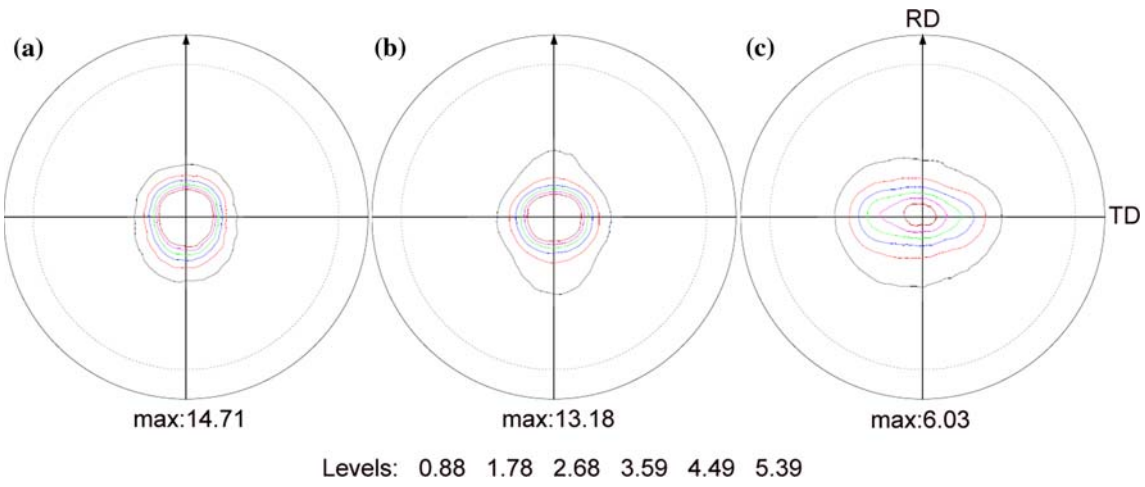

Fig. 5 The (0002) pole figures of **a** NRed, **b** 1P-ECARed, and **c** C-ECARed sheets

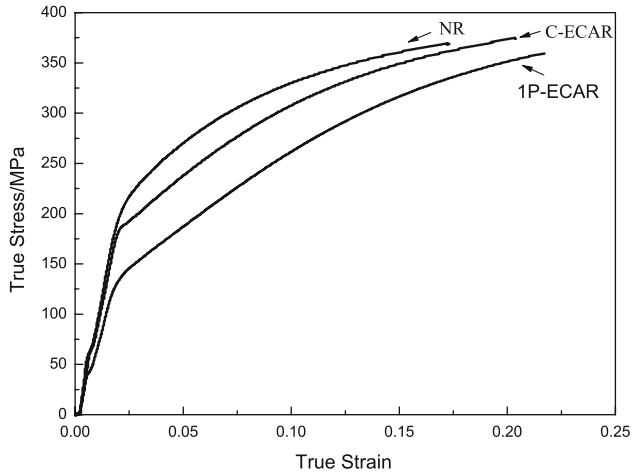

Fig. 6 The tensile curves of the samples in RD during the uniform plastic deformation

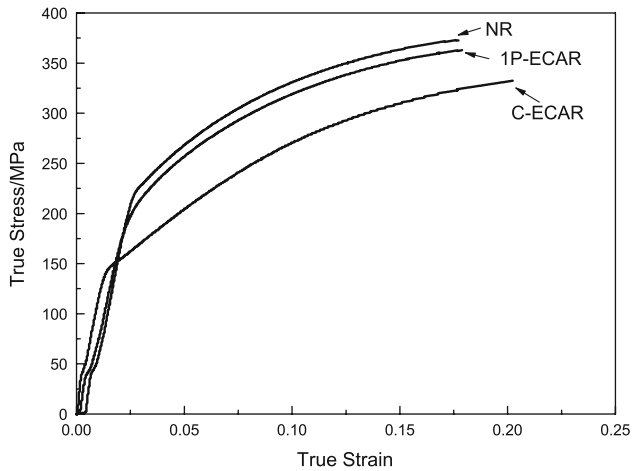

Fig. 7 The tensile curves of the samples in TD during the uniform plastic deformation

Table 1 Tensile data of the as-rolled sheets in different directions

Sample	Tensile direction	σ_s/MPa	σ_b/MPa	δ/%	σ_s/σ_b	n
NR	RD	202	303	23.5	0.67	0.27
	TD	213	312	22.3	0.68	0.28
1P-ECAR	RD	140	281	29.5	0.50	0.44
	TD	188	297	24.0	0.63	0.29
C-ECAR	RD	177	300	27.5	0.59	0.36
	TD	145	272	26.5	0.53	0.33

1P-ECAR along RD, the σ_s in RD decreases dramatically from 202 to 140 MPa. And after rotating the sheets for 90° followed by C-ECAR process, the σ_s in RD reduces to 177 MPa from 188 MPa of the 1P-ECARed sheets in TD. It can be suggested that ECAR could markedly decrease the yield strength in RD. And the variation of σ_b is not as sharp as σ_s, from 303 to 281 MPa after 1P-ECAR, and from 297 to 300 MPa after C-ECAR process. The δ along RD of the 1P-ECARed sheets increases to 29.5% from 23.5% of the NRed sheets, and the C-ECAEed samples have almost the same δ along RD and TD, which are 27.5 and 26.5%, respectively. Compared with the NRed sheets, the tensile properties of the C-ECARed sheets have been improved along both the RD and TD.

The strain hardening exponent, n value, was calculated from the true stress–true strain curves during the uniform plastic deformation, according to the formula

$$\ln \sigma = n \ln \varepsilon + \ln k,$$

where σ is the true stress, ε is the true strain, k is a constant, and n is the strain hardening exponent. After 1P-ECAR, the n value in RD notably increases, up to 0.44, while in TD the n value had no significant change. After C-ECAR, the n values increase in both the RD and TD compared with the NRed sheets, and the values in RD and TD are closer than that of the 1P-ECARed sheets. The increase in n value suggests that the ECAR sheets should show obviously strain hardening behavior. From Table 1 it can also be seen that yield ratio σ_s/σ_b decreases and n value increases after ECAR. This trend of σ_s/σ_b and n value means that the uniform plastic deformation would increase (see Figs. 6 and 7).

Figure 8 gives the SEM images of fracture surfaces of the tensile samples. The NRed and C-ECARed samples both show ductile fracture. The dimples in the C-ECARed sample are slightly deeper than that in the NRed sample. There are several tearing ridges (arrow 1 in Fig. 8b), from which cracks may initiate (arrow 2 in Fig. 8b). Cracks can also be generated by the connecting the adjacent dimples (arrows 3 and 4 in Fig. 8b). These microcracks can readily propagate to form macrocracks and lead to fracture of the tensile sample.

Discussion

Shear stress is supplied to the sheet during ECAR, which results in the texture weakening, as shown in Fig. 5. As the basal planes of most grains in the NRed sheets almost parallel to the rolling plane, grains are compressed along c-axis during rolling and $\{10\bar{1}1\}$ contraction twinning system is initiated. Since $\{10\bar{1}2\}$ extension twinning system is the preferential twinning mechanism in magnesium alloy, a few $\{10\bar{1}2\}$ twinning occurs in some "soft" grains. While during C-ECAR, a large number of basal planes deviate from the rolling plane, and the $\{10\bar{1}2\}$ extension twinning system is preferred to activate.

As is well known, basal slip and $\{10\bar{1}2\}$ twinning are the dominating mechanism to accommodate plastic

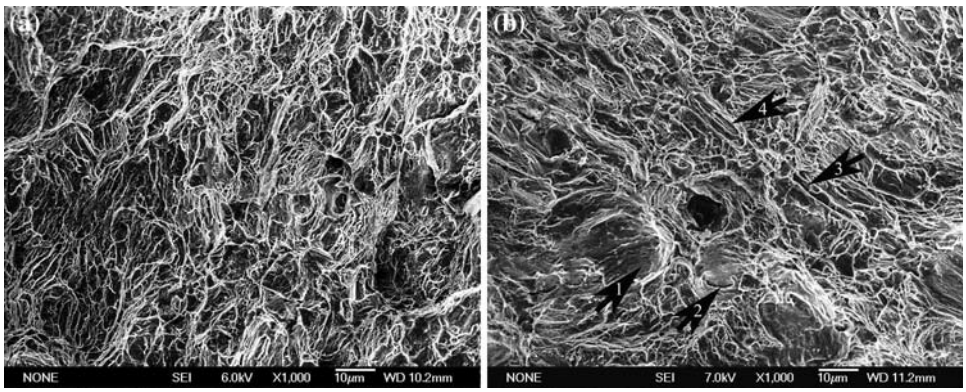

Fig. 8 The SEM images of tensile fractures of **a** NRed **b** C-ECARed sheets in RD

deformation of magnesium alloy at room temperature. When tensioned in the rolling plane, as a consequence of grain re-orientation, the Schmid factor of basal ⟨a⟩ slip system in the ECARed sheets is higher than that in the NRed sheets, thus the basal slip is more prone to initiate in the ECARed sheets, therefore lower yield strength can be obtained. Moreover, most grains are compressed along *c*-axis when samples tensioned along both RD and TD in the NRed samples, $\{10\bar{1}2\}$ twinning is hard to initiate. While the activation of $\{10\bar{1}2\}$ twinning is easier in the ECARed samples due to the tilting texture. It has been revealed that the activation of $\{10\bar{1}2\}$ twinning plays an important role in the yield strength of magnesium alloys [24, 25]. Therefore, the easier initiation of basal slip and $\{10\bar{1}2\}$ twinning caused by texture weakening makes substantial contribution to the lower yield strength in the ECAR direction.

Though the grains are finer, the yield strength of the annealed ECARed samples is lower than that of the annealed NRed samples in the tensile test (shown in Figs. 3, 6, 7 and Table 1), which means that the hardening effect of a fine grain size might be lower than the softening effect of the weakened new texture of the processed samples. Similar phenomenon during ECAP on AZ31B alloy has been reported by Agnew et al. [26]. Furthermore, the basal planes in the C-ECARed samples spread much wider to TD than to RD, which leads to the heterogeneity of yield strengths along the two directions, 145 MPa in TD and 177 MPa in RD, respectively (see Fig. 5c and Table 1). This anisotropy in the two directions also indicates that the texture has great effect on the yield strength of magnesium alloys. The weakened texture also improves the ductility of ECARed samples.

Higher strain hardening of the annealed ECARed sheets (see Fig. 6, 7 and Table 1) would be a consequence of the numerous dislocation piles-up on the more fine-grain boundaries and twinning boundaries. The more slip and slip–twinning interaction would be another reason for severe strain hardening [24, 25].

Conclusions

The AZ31 magnesium alloy sheets were fabricated by a novel ECAR processing. The microstructure, texture, and mechanical properties of the 1P-ECARed and C-ECARed sheets were compared with the NRed sheets. The following conclusions can be drawn from this study:

(1) ECAR processing can weaken the basal plane texture of magnesium alloy sheets due to the shear stress applied by the ECAR die, which can result in obviously improvement of mechanical properties. The yield ratio σ_s/σ_b decreases and strain hardening exponent n increases along RD during ECAR, which means that the uniform plastic formability is enhanced. After C-ECAR, the mechanical properties along both the RD and TD are improved.

(2) Twinning plays an important role in the ECAR processing. The most frequent twinning types in the NRed and ECARed sheets are different, which are fine $\{10\bar{1}1\}$ contraction twinning, and coarse $\{10\bar{1}2\}$ extension twinning, respectively. This difference can be attributed to the grain orientation. The basal planes rotate a relatively larger angle from rolling plane in the ECARed sheets, thus the $\{10\bar{1}2\}$ twinning is more prone to initiate. The easier activation of $\{10\bar{1}2\}$ twinning and basal ⟨a⟩ slip leads to the lower yield strength of the ECARed sheets.

(3) DRX during the rolling process has great effect on the microstructure of the as-deformed and annealed sheets. The annealed C-ECARed sheets have significant finer and homogenous grains than the annealed NRed sheets, which is attributed to the rarely DRX process during ECAR. The average grain sizes of the annealed C-ECARed samples and the NRed samples are 14 and 24 μm, respectively.

Acknowledgements The research described in this paper was supported by the Program for New Century Excellent Talents in University of Ministry of Education of China (NCET-06-0701), the

Doctoral Program of Higher Education of China (20070532087) and the Natural Science Foundation Project of China (50844034).

References

1. Lee BH, Reddy NS, Yeom JT, Lee CS (2007) J Mater Process Technol 187–188:766
2. Pérez-Prado MT, del Valle JA, Ruano OA (2005) Mater Lett 59:3299
3. Wang SC, Chou CP (2008) J Mater Process Technol 197:116
4. Garcés G, Müller A, Oñorbe E, Pérez P, Adeva P (2008) J Mater Process Technol 206:99
5. Suwas S, Gottstein G, Kumar R (2007) Mater Sci Eng A 471:1
6. Nagasekhar AV, Tick-Hon Y, Seow HP (2007) J Mater Process Technol 192–193:449
7. Kai M, Horita Z, Langdon TG (2008) Mater Sci Eng A 488:117
8. Chen YJ, Wang QD, Roven HJ, Karlsen M, Yu YD, Liu MP, Hjelen J (2008) J Alloy Compd 462:192
9. Pérez-Prado MT, del Valle JA, Ruano OA (2004) Scripta Mater 51:1093
10. Guo Q, Yan HG, Chen ZH, Zhang H (2006) Trans Nonferrous Met Soc China 16:922
11. Rajinikanth V, Arora G, Narasaiah N, Venkateswarlu K (2008) Mater Lett 62:301
12. Matsubara K, Miyahara Y, Horita Z, Langdon TG (2005) Acta Mater 51:3073
13. Watanabe H, Mukai T, Ishikawa K, Higashi K (2002) Scripta Mater 46:851
14. Lee JC, Seok HK, Han JH, Chung YH (2001) Mater Res Bull 36:997
15. Lee JC, Seok HK, Suh JY (2002) Acta Mater 50:4005
16. Nam CY, Han JH, Chung YH, Shin MC (2003) Mater Sci Eng A 347:253
17. Huh MY, Lee JP, Lee JC (2004) Mater Sci Tech 20:819
18. Park JW, Kim JW, Chung YH (2004) Scripta Mater 51:181
19. Kang HG, Lee JP, Huh M, Engler O (2008) Mater Sci Eng A 486:470
20. Cheng YQ, Chen ZH, Xia WJ, Zhou T (2007) J Mater Process Technol 184:97
21. Chen ZH, Cheng YQ, Xia WJ (2007) Mater Manuf Process 22:51
22. Cheng YQ, Chen ZH, Xia WJ (2007) J Mater Sci 42:3552. doi: 10.1007/s10853-007-1559-0
23. Cheng YQ, Chen ZH, Xia WJ (2007) Mater Charact 58:617
24. Wang YN, Huang JC (2007) Acta Mater 55:897
25. Chino Y, Kimura K, Hakamada M, Mabuchi M (2008) Mater Sci Eng A 485:311
26. Agnew SR, Horton JA, Lillo TM, Brown DW (2004) Scripta Mater 50:377